

DOI: 10.1002/adem.200600206

Experimental Measurement and Computer Simulation of Galvanic Corrosion of Magnesium Coupled to Steel**

By Jimmy X. Jia, Guangling Song and Andrej Atrens*

The study of the galvanic corrosion of magnesium becomes increasingly important as the use of magnesium alloys increases rapidly in the auto and aerospace industries due to their advantages of light-weight, adequate mechanical properties and moderate cost. Corrosion, however, limits the application of magnesium alloys.^[1-7] A number of different mechanisms are important for the corrosion.^[8-14] But galvanic corrosion is probably the most important for magnesium because magnesium is the most active structural metal and consequently may suffer serious corrosion when joined to all other common metals of construction, such as aluminum or steel.^[1,2,15] Fasteners and their galvanic corrosion is of major concern in automotive applications.^[16-18] Skar^[17] showed that 6000 series aluminum alloy fasteners caused negligible galvanic corrosion of magnesium in the salt spray test. However, steel fasteners are desired for many applications due to their inherently better mechanical properties. Poor compatibility with magnesium was shown by aluminium-coated steel fasteners^[18] whereas steel fasteners with zinc or tin-zinc alloy coatings were compatible with magnesium in salt-water exposure.^[16] To be able to design a structural component, incorporating galvanic corrosion, it is useful to be able to simulate the galvanic corrosion distribution qualitatively. The research presented in this paper has been undertaken as part of a program to explore that aim. The total corrosion in the area of galvanic corrosion can be considered to be made up of the following two components: (1) galvanic corrosion and (2) self corrosion. The galvanic corrosion is that part of the corrosion, which is directly caused by the coupling of the magnesium to a steel fastener. The self-corrosion is defined as the extra corrosion. Both the galvanic corrosion and the self-corrosion may take the form of more or less general corrosion, or the form of localized corrosion or pitting corrosion.

Prior studies of galvanic corrosion of magnesium have been scarce. The earliest study, started in the 1950s by Teeple,^[19] investigated the influence of location and climate. This study revealed that different locations produced different corrosion rates because of the different electrolyte properties of the condensed film on the metal surface.^[19] Atmospheric galvanic corrosion could be detrimental for magnesium in one location whilst it was almost harmless in another location. This provided helpful information to select magnesium for a particular location. However, the study was time consuming. It is often not practical to wait years to have the test results for each particular service location. Limited studies have addressed the effect of electrolyte on the galvanic corrosion of magnesium. More effort has been focused on general corrosion, particularly on the influence of the ion species in solution, and the influence of cathodic impurity elements in the alloy.^[20-28] The influence of the electrolyte involves many factors such as pH, composition, concentration of the ions and the conductivity of the electrolyte. The influence of conductivity on galvanic corrosion has been studied in terms of "macroscopic" and "microscopic" galvanic cells,^[29] and in terms of the Wagner number.^[30,31] Recent research revealed the "alkalization", "passivation" and "poisoning" effects during salt spray exposure.^[15] In addition, the galvanic cell geometry significantly influences the galvanic corrosion behaviour. Geometrical factors include the anode/cathode area ratio, the insulation distance between the anode and cathode, electrolyte film thickness and the shapes of the anode and cathode.^[32] Furthermore, there could be more than one galvanic couple such as many steel fasteners for one magnesium part, and there could be an interaction of the current caused by each galvanic couple.

Various methods have been employed to measure galvanic corrosion. Galvanic corrosion of magnesium has been measured in terms of weight loss and pitting depth.^[33-37] The weight loss and pitting depth methods actually measure the total corrosion rate, which is the sum of general and galvanic corrosion. These methods are not accurate in terms of just the galvanic corrosion. The method of surface potential scanning provides the surface potential distribution,^[38] but the potential is not directly related to the galvanic corrosion rate. The present study measured the galvanic current, which directly relates to the galvanic corrosion rate.

The BEM is a relatively new numerical method and is becoming more important with recent developments in computer technology. Numerical methods have been utilized in

[*] Dr J. X. Jia, Dr G. Song, Prof. A. Atrens
CRC for Cast Metals Manufacturing (CAST)
Division of Materials, School of Engineering
The University of Queensland
St Lucia, QLD 4072, Australia
E-mail: a.atrens@minmet.uq.edu.au

[**] The authors would like to acknowledge the financial support of the Cooperative Research Centre for Cast Metals Manufacturing (CAST). CAST was established and is funded in part by the Australian Government's Cooperative Research Centres Program.

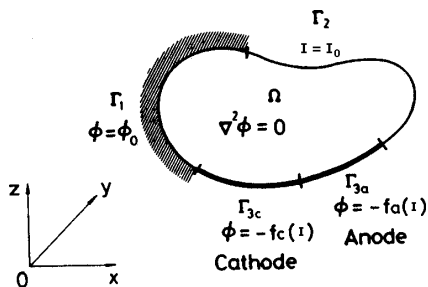


Fig. 1. Basic equations and boundary conditions for the BEM model.

galvanic corrosion analysis since the early 1980's. The application of BEM to galvanic corrosion analysis has been reviewed by Adey and Niku,^[39] Munn,^[40] Aoki^[41,42] and Brebbia.^[43] Adey^[39] stated that BEM was suitable for modeling corrosion, and that computer simulation of galvanic corrosion could be undertaken with confidence with commercial programs like BEASY. Our preliminary research^[44] showed that the BEM program BEASY provided calculated values in agreement with analytical approaches and FEM calculations. Most of the previous studies have also reported agreement between modeling predictions and experimental measurements for the galvanic current distribution.^[45-52] In contrast, Ault and Meany^[53] concluded: a) "the deepest pit was not immediately adjacent to the cathodic metals that most mathematical models predict"; b) "the mathematical model only can provide a order of magnitude estimation of galvanic current flow"; and c) "the mathematical model can neither accurately predict long term current distribution nor the magnitude of pitting corrosion". These conclusions are of particular significance for the present study on the galvanic corrosion of magnesium because localized corrosion is often the form of corrosion of magnesium in practical solutions as typified by 5% NaCl solution. Thus evaluation of BEM is necessary to reveal the potential challenges in the prediction of galvanic corrosion of magnesium using BEM.

The aim of this study was to provide insight into galvanic corrosion prediction and prevention for real auto, aerospace or marine components. The environment was taken into account using the experimentally measured polarization curve as the boundary condition for the BEM model. The BEM model calculations were compared with the experimentally

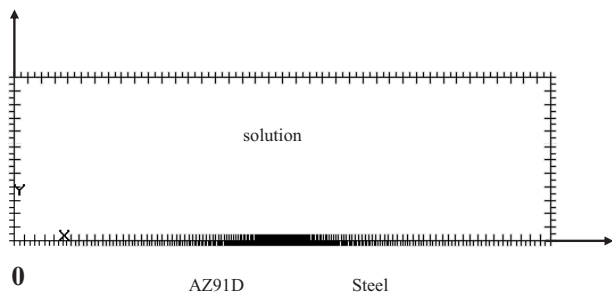


Fig. 2. Schematic illustration of the detail of the BEM mesh for a one dimension (1D) galvanic couple, i.e. as for the geometries presented in Figures 4 and 5.

measured galvanic current. The present study investigated the influence of geometry on the galvanic current distribution of magnesium in contact with steel in a 5% NaCl solution. The aim was to evaluate the galvanic corrosion of magnesium for various area ratios of anode/cathode, solution film thickness, the insulation spacing and the interaction of two galvanic couples. In addition, the galvanic corrosion of AZ91D coupled to a steel fastener was studied. This research could provide helpful information for magnesium structure design and optimization in the auto and the aerospace industry

Theory

Galvanic Current Distribution

The initial steady state current distribution is produced as a result of the solution resistance and the potential difference between the anode and the cathode surfaces. The corrosion potential of magnesium and steel in the same electrolyte are different, which results in a current to flow through the electrolyte when the metals are brought into contact. The equation governing the current flow and the potential distribution in the electrolyte can be derived from first principles. The continuity equation (charge conservation) requires that the current per unit volume, I , relates to the charge, q , by.^[54]

$$-\nabla I = \frac{\partial q}{\partial t} \tag{1}$$

For a system in steady state, $\partial q/\partial t=0$. Taking into account the relationship of electric field intensity, E ,

$$E = -\nabla\phi \tag{2}$$

and Ohms law,

$$I = KE \tag{3}$$

where K is the conductivity of the electrolyte, the continuity equation transforms to

$$\nabla K \nabla \phi = 0 \tag{4}$$

For an electrolyte with uniform, isotropic conductivity, K is a constant, so that,

$$\nabla^2 \phi = 0 \tag{5}$$

Therefore, for a uniform, isotropic electrolyte, the potential obeys Equation 5, which is the Laplace equation. The current density at any point inside the electrolyte can be evaluated using:

$$I_{xi} = -K \frac{\partial \phi}{\partial x_i} \tag{6}$$

where I_{xi} is the current density in the x_i direction, ϕ is the potential.

Boundary element method (BEM)

The mathematical formulation has been described by Adey et al.^[55] for a uniform, isotropic electrolyte domain Ω as illustrated in Figure 1. The Laplace equation (Eq. 5) is solved using the following boundary conditions:

$$\phi = \phi_0, \text{ on } \Gamma_1, \quad (7)$$

$$I = I_0, \text{ on } \Gamma_2, \quad (8)$$

$$I_a = f_a(\phi), \text{ on } \Gamma_{3a}, \quad (9)$$

$$I_c = f_c(\phi), \text{ on } \Gamma_{3c}, \quad (10)$$

where $\Gamma = (\Gamma_1 + \Gamma_2 + \Gamma_{3a} + \Gamma_{3c})$ is the entire surface of the electrolyte domain Ω , I is the current density across the boundary, ϕ is the potential, ϕ_0 and I_0 are given constant values of potential and current density respectively, and $f_a(\phi)$ and $f_c(\phi)$ are functions that describe the anode and cathode electrode kinetics respectively.

When using the boundary element method to solve the Laplace equation, the residual weighting function is chosen to minimize the error. The boundary integral expression was derived as Equation 11 by reducing the integral equation.

$$c(y)\phi(y) + \int_{\Gamma} \phi(x)I^*(y,x)d\Gamma(x) = \int_{\Gamma} I(x)\phi^*(y,x)d\Gamma(x) \quad (11)$$

where ϕ^* and I^* are the fundamental solutions. The boundary of the electrolyte is divided into fine boundary elements that are non-overlapping and cover the whole of the boundary. Equation 11 can be rewritten as

$$c_i\phi_i + \int_{\Gamma} \phi I^* d\Gamma = \int_{\Gamma} I \phi^* d\Gamma \quad (12)$$

Since G has been approximated by N elements, Equation 12 becomes

$$c_i\phi_i + \sum_{j=1}^N \int_{\Gamma_j} \phi I^* d\Gamma = \sum_{j=1}^N \int_{\Gamma_j} I \phi^* d\Gamma \quad (13)$$

where \int_{Γ_j} denotes integration over element j . The equations for all elements can be assembled into a system of linear simultaneous equations, which is expressed in a matrix form as follows:

$$H \phi = G I \quad (14)$$

where H and G are problem influence matrices, and ϕ and I represent potential and current density vectors respectively. The size of the system of equations is defined by the number of nodes. Partitioning the ϕ and I into those nodes which

form the anode and the cathode regions and applying the boundary condition, Equation 9 and Equation 10, gives

$$\begin{bmatrix} h_{aa} & h_{ac} \\ h_{ca} & h_{cc} \end{bmatrix} \begin{bmatrix} \phi_a \\ \phi_c \end{bmatrix} = \begin{bmatrix} g_{aa} & g_{ac} \\ g_{ca} & g_{cc} \end{bmatrix} \begin{bmatrix} f_a(\phi_a) \\ f_c(\phi_c) \end{bmatrix} \quad (15)$$

Equation 15 is solved by an iteration method. The boundary conditions provide the potential

$$\begin{bmatrix} \phi_a \\ \phi_c \end{bmatrix}$$

and the current

$$\begin{bmatrix} I_a \\ I_c \end{bmatrix} = \begin{bmatrix} f_a(\phi_a) \\ f_c(\phi_c) \end{bmatrix}$$

Solution of Equation 15 gives

$$\begin{bmatrix} \phi_a^n \\ \phi_c^n \end{bmatrix}$$

at the n^{th} iteration for all metal elements: when

$$\begin{bmatrix} \phi_a^n \\ \phi_c^n \end{bmatrix} - \begin{bmatrix} \phi_a^{n-1} \\ \phi_c^{n-1} \end{bmatrix} \leq \xi \quad (16)$$

where ξ is the tolerance. This provides the calculated values of the potential

$$\begin{bmatrix} \phi_a^n \\ \phi_c^n \end{bmatrix}$$

throughout the boundary. The galvanic current density can be calculated using Equations 9 and 10.

BEASY Implementation of BEM

This study used the boundary element program BEASY. The boundary was divided into AZ91D elements and steel elements as illustrated in Figures 2 and 3. The input param-

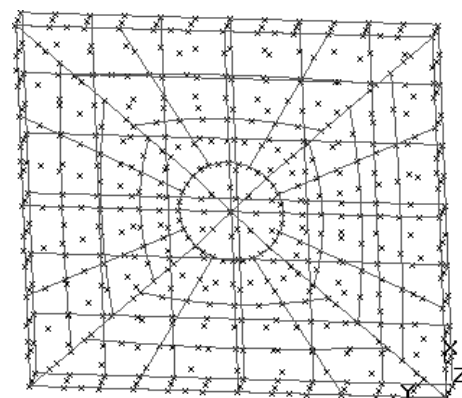


Fig. 3. Schematic of the mesh for the BEM model for a steel fastener modelled as a steel insert (diameter = 30 mm) in a horizontal AZ91D sheet covered with an electrolyte of uniform depth.

ters included the physical geometry of the galvanic couple, the electrolyte conductivity and the boundary conditions: i.e.

$$\begin{bmatrix} \phi_{a0} \\ \phi_{c0} \end{bmatrix}$$

and

$$\begin{bmatrix} f'_a(\phi) \\ f'_c(\phi) \end{bmatrix}$$

where ϕ_{a0} was the open circuit potential of the anode; ϕ_{c0} was the open circuit potential of the cathode; $f'_a(\phi)$ was the function used in BEASY to represent the anode metal polarization curve given by equation (9); similarly $f'_c(\phi)$ was the function representing the cathode metal polarization curve. The polarization curve was introduced using the the piecewise linear approach. The polarization curve was divided into small segments, such that each segment was approximated by a linear relationship between the potential and current given by:

$$I = f(\phi) = k(\phi - \phi_a) + I_a \tag{17}$$

where k , ϕ_a and I_a were known constants for each line segment.

Experimental Procedure

Electrolyte

The 5% NaCl solution used represents a severe corrosive environment such as a marine environment or the environment near the beach. The solution was made with analytical reagents and deionized water. The conductivity was measured using a platinum conductivity cell to be 79500 $\mu\text{S}\cdot\text{cm}$.

Galvanic Corrosion (1D) Assembly (GCA)

The high pressure die cast (HPDC) magnesium alloy AZ91D and mild steel were used. AZ91D was chosen because it is the most widely used magnesium alloy. AZ91D contains about 9% aluminium and less than 1% zinc. Mild steel is

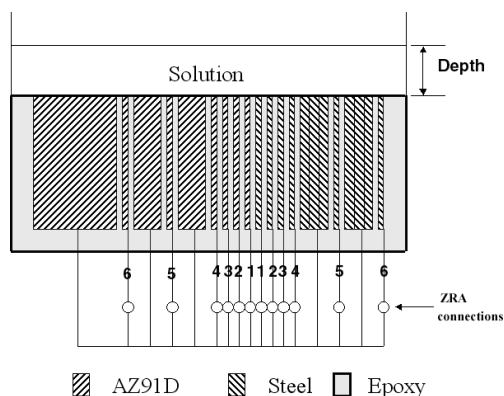


Fig. 4. Multi-electrode Mg-steel galvanic corrosion assembly (GCA) for the study of 1D galvanic corrosion.

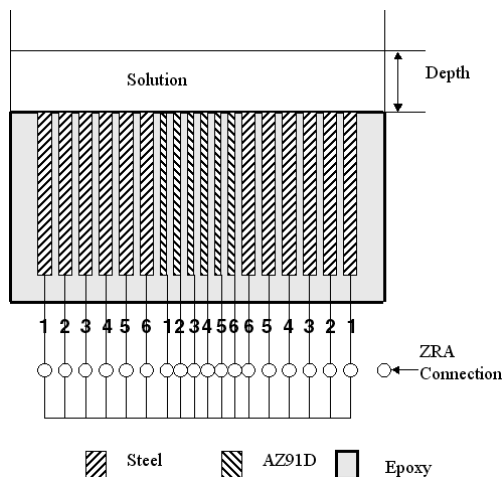


Fig. 5. Galvanic corrosion interaction assembly.

the metal most used in industry.^[56] The metal plates were molded in epoxy as shown in Figure 4 following the prior design.^[15] The width of the plates (i.e. the distance into the plane of the cross-section) was much greater than the thickness, allowing idealized study of the galvanic corrosion in one dimension (1D). The insulation distance was 0.5 mm between adjacent plates. The galvanic current was measured for six plates of AZ91D and six plates of mild steel. The surface area exposed to the solution of each metal plate was 1.2 mm (thickness) and 35 mm (width) (42 mm² surface area). The galvanic cell size could be changed by connecting or disconnecting some of the metal plates. The solution depth was arbitrarily chosen as 10 mm except for the cases that studied the influence of solution depth. The surface of the electrodes of the specimen was polished using 1200 # silicon carbide sandpaper, washed with water and ethanol and dried. The specimen was immediately immersed in the solution. A multi-channel Zero Resistance Ammeter (ZRA) was used to measure the galvanic currents passing through each electrode as a function of time as illustrated in Figure 4.

Galvanic Interaction Assembly

The assembly of steel-AZ91D-steel (St_Mg_St) for the study of galvanic interaction consisted of twelve mild steel plates and six AZ91D plates as shown in Figure 5. The sur-

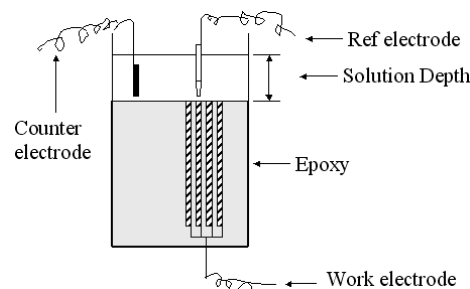


Fig. 6. Schematic of arrangement for measuring polarization curves.

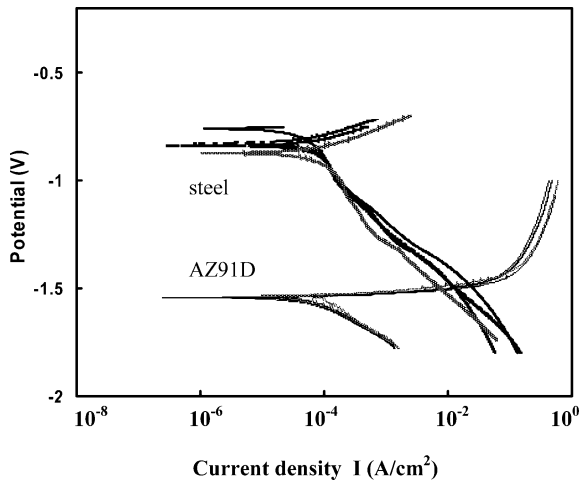


Fig. 7. Potentiodynamic polarization curves for AZ91D and steel in 5% NaCl solution using a scan rate of 2 mV/s. Solution depth was 10 mm.

face area of each plate exposed to the electrolyte was 56 mm² for each steel plate with 1.6 mm (thickness) and 35 mm (width) and 42 mm² for each AZ91D plate with 1.2 mm (thickness) and 35 mm (width). The connections for the measurement of the galvanic current for the galvanic corrosion interaction specimen could be made as shown Figure 5. This arrangement is designated St_Mg_St, and allows the measurement of the interaction of the galvanic corrosion from the galvanic couple on the left (*i.e.* St_Mg) and from the galvanic couple on the right side (*i.e.* Mg_St). In addition, the electrical connections could be made to separately measure the galvanic currents from the left hand side couple (St_Mg) or alternatively separately measure the galvanic currents associated with the right hand side couple (Mg_St).

Idealised Fastener

HPDC AZ91D and mild steel were the test materials. Each assembly consisted of an 11 cm × 12 cm plate of AZ91D containing a mild steel circular insert in the center of the plate.

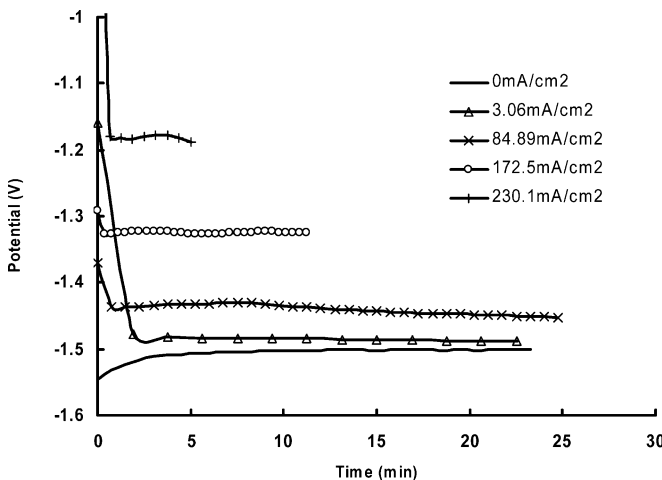


Fig. 8. Galvanostatic measurement of potential versus time for AZ91D in 5% NaCl solution at room temperature.

The diameters of the mild steel inserts were 5 mm, 10 mm and 30 mm. The steel was insulated from the AZ91D by a thin layer of Teflon and molded in resin. The AZ91D plate and steel electrode were electrically connected by a wire and formed a galvanic couple.

After 48 hrs of emersion in a 5% NaCl solution to a depth of 10 mm, the corrosion product was removed from the surface of each specimen. The corrosion morphology was recorded. Each specimen was sectioned into 8 pie-shaped pieces. The corroded area on each cross section was measured in 1 mm sections using an optical microscope and the Leica Qwin image analysis software. The average corrosion rate for each sample was calculated by integrating the damage depth along the length of each cross section.

Polarization Curve Measurement

Figure 6 presents the experimental arrangement for the measurement of the potentiodynamic and galvanostatic polarization curves. The measurement of galvanostatic polarization curves used the potentiodynamic curves as a guide for the current density values. For each applied constant current density, the potential was measured with time to give the galvanostatic polarization curves at 5 to 10 min for the 5% NaCl solution. The solartron 1287 electrochemical interface was used to measure the potentiodynamic polarization curves using an Ag/AgCl reference electrode. The solution resistance was measured using the 1255B Frequency Response Analyzer and all polarization curves have been corrected for the potential drop caused by the solution resistance.

Results

Polarization Curves

Potentiodynamic polarization curves of AZ91D and steel were reproducible as shown by Figure 7. The four repeated measurements showed reasonable agreement. Hack and Scully^[57] indicated that it was necessary to use long-term po-

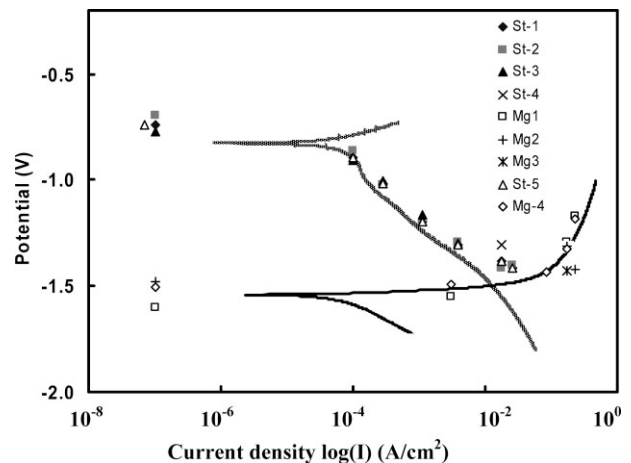


Fig. 9. Galvanostatic polarization curve measurements in 5% NaCl solution. Curves represent typical potentiodynamic polarization curves, at scan rate of 2 mV/s.

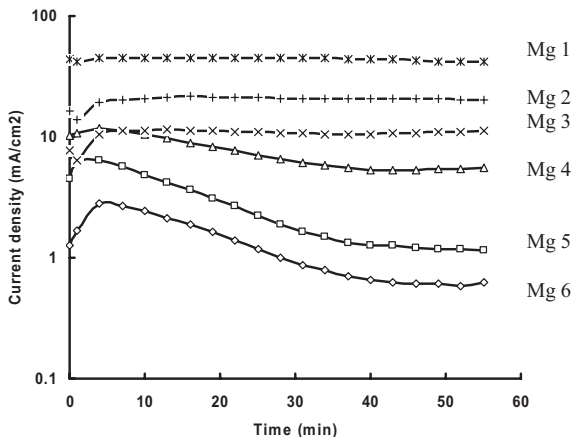


Fig. 10. Galvanic current density at AZ91D electrodes (designated Mg 1 to Mg 6) in 5% NaCl solution.

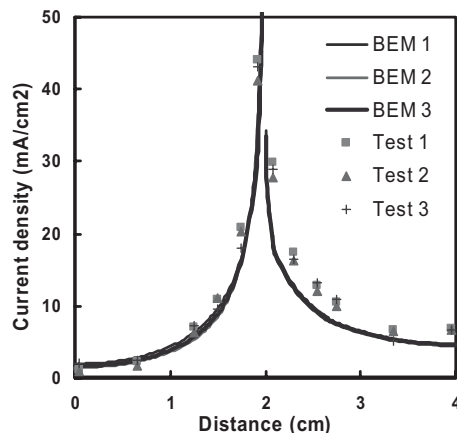


Fig. 12 Comparison of BEM model (curves) and experiment data (data points) for an area ratio of A/C of 1:1. $d = 10$ mm. AZ91D is on the left, steel on the right hand side, and similarly for figures 13, 14 and 19.

larization curves to adequately predict the galvanic corrosion, and as a consequence, galvanostatic curves were measured. The particular current density values, chosen based on the potentiostatic polarization curves, were applied and the resulting potential was measured as shown by typical curves in figure 8. In each case, multiple measurements were made. The potential of AZ91D and steel rapidly reached steady state values. Intense hydrogen evolution on the surface of steel and AZ91D stirred up the corrosion product inside the solution and there was no stable deposited film on the surface of AZ91D. Approach to steady state was rapid, steady state had been reached by 5 to 10 min, whereafter there was little further change. Consequently the polarization curves represent steady state and thus maybe used as the boundary conditions for the BEM model to predict steady state galvanic corrosion. Figure 9 shows the galvanostatic polarization curves compared with the potentiodynamic polarization curves for AZ91D and steel. The data for the two methods were within experimental error.

Galvanic Current Measurements

The measurement of galvanic current using the GCA illustrated in Figure 4 for electrodes of AZ91D and steel in 5% NaCl solution are shown in Figures 10 and 11. Galvanic currents of electrodes Mg1 to Mg3 exhibited relatively constant high values whereas the galvanic currents of electrodes Mg4 to Mg6 initially decreased and then approach steady state values as shown in Figure 10. This initial decrease is interpreted as a result of the corrosion product deposit contributing some protection on electrodes of Mg4 to Mg6, but there was little protection on electrodes Mg1 to Mg3, which suffered intense dissolution. The current in the steel electrodes also decreased slightly as shown in Figure 11. The total current from the AZ91D electrodes (positive) should be equal to that from the steel electrodes (negative). The sum of the total current from the AZ91D and steel oscillated around the zero. There was an initial transient, whereafter the sum of the total current gradually tended to be stable around zero as the galvanic corrosion became stabilized.

The surface of the specimen was observed after the galvanic corrosion test. There was severe pitting on the surface of the AZ91D electrodes with the pitting being severest for elec-

The surface of the specimen was observed after the galvanic corrosion test. There was severe pitting on the surface of the AZ91D electrodes with the pitting being severest for elec-

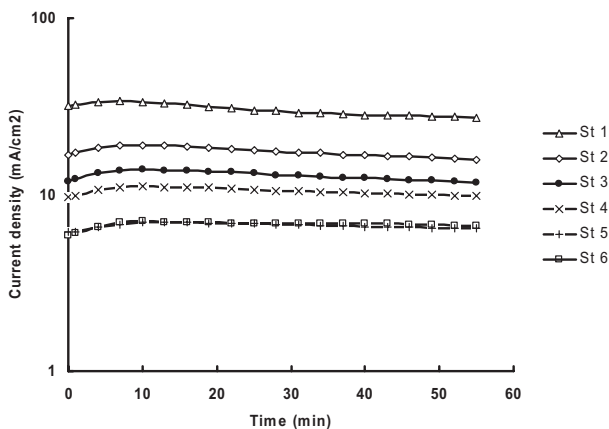


Fig. 11. Galvanic current density at steel electrodes (designated St 1 to St 6) in 5% NaCl solution.

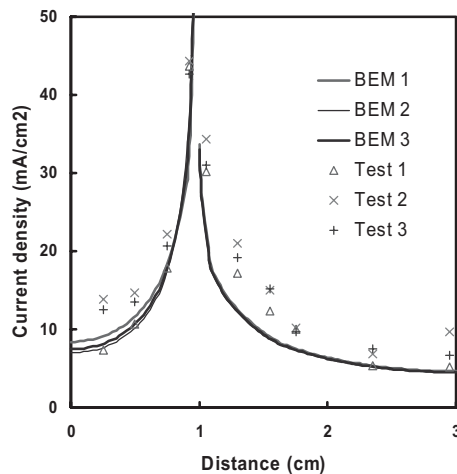


Fig. 13 Comparison of BEM model (curves) and experiment data (data points) for an area ratio of A/C of 1:2. $d = 10$ mm.

Table 1. Boundary conditions in 5% NaCl solution used for BEM calculations, related to the data of Figure 7.

	Current density (mA/cm ²)	Potential (V)		
		BEM 1	BEM 2	BEM 3
Steel	0.000	-0.771	-0.695	-0.741
	0.100	-0.906	-0.863	-0.896
	0.290	-1.003	-1.021	-1.018
	1.100	-1.165	-1.202	-1.194
	3.860	-1.298	-1.296	-1.305
	17.700	-1.307	-1.413	-1.386
	25.400	-1.418	-1.403	-1.417
AZ 91 D	0.000	-1.480	-1.600	-1.506
	-3.058	-1.430	-1.550	-1.492
	-84.880	-1.431	-1.431	-1.431
	-172.500	-1.310	-1.290	-1.325
	-230.100	-1.420	-1.170	-1.183

trode Mg1. There was no obvious deposit film on the surface of the AZ91D and steel electrodes.

Effect of Area Ratio of Anode/Cathode

Figures 12 and 13 illustrate the galvanic current distribution for the AZ91D-steel galvanic couple in 5% NaCl solution for various area ratios of anode/cathode measured using the GCA illustrated in Figure 4. The current distributions from the BEM model are compared with the experimental measurement for an area ratio of anode/cathode of 1:1 in Figure 12, and of 1:2 in Figure 13. The area ratio of 2:1 was also studied. The BEM model used the boundary conditions as given in Table 1. There was reasonable agreement between

the BEM model and the experimental measurements. As the area ratio was changed from 2:1 to 1:1 to 1:2 the galvanic current of the AZ91D electrode increased from 33 mA/cm² to 44 mA/cm² for electrode Mg1, from 14 mA/cm² to 22 mA/cm² for electrode Mg2, from 11 mA/cm² to 17 mA/cm² for electrode Mg3 and from 10 mA/cm² to 14 mA/cm² for electrode Mg4. The galvanic current of the AZ91D electrodes increased with the decrease of area ratio of anode/cathode as expected. The influence of area ratio of anode/cathode on the galvanic current distribution for AZ91D-steel in 5% could be reasonably predicted using the BEM approach.

Influence of Solution Film Thickness

Figures 12 and 14 present the galvanic current distributions from the BEM model compared with the experimental measurements for film thickness values of 10 mm and 1 mm respectively. (A film thickness of 3 mm was also studied and gave results intermediate between the other two cases). The BEM model used the boundary conditions as given in Table 1. The galvanic current of each electrode increased with the increase of film thickness

as expected because the increase of the film thickness resulted in a larger area for the current pass and thus reduced the solution resistance against the current flow. There was reasonable agreement both in trend and in current value between the BEM model and the experimental measurement.

Galvanic Corrosion Interaction

Figure 15 presents the galvanic current distribution for both the BEM model and the experimental measurements for the galvanic corrosion interaction assembly, Figure 5. There was a reasonable agreement between the BEM model and the experimental results. Figure 16 presents both (a) the galvanic

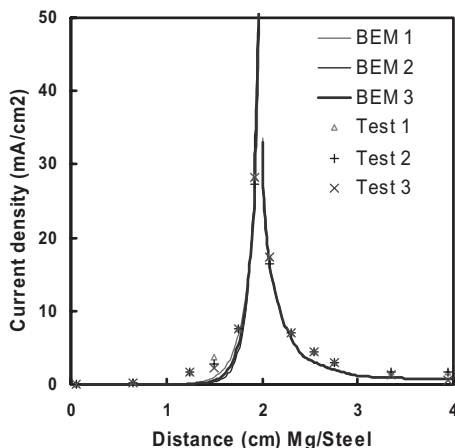


Fig. 14. Comparison of galvanic current distribution between the BEM model (curve) and experimental measurements (data points), d=1 mm.

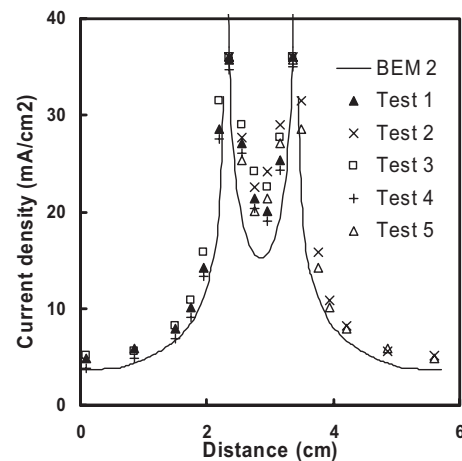


Fig. 15. Comparison between the BEM model (curves) and the experimental measurements (data points) of galvanic current for the galvanic corrosion interaction specimen (St_Mg_St) as illustrated in Figure 5, d=10 mm.

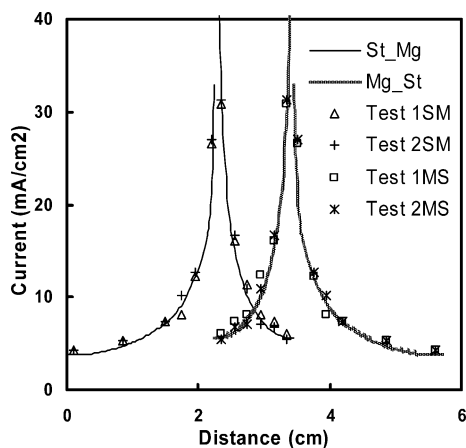


Fig. 16. Comparison between the BEM model (curves) and the experimental measurements (data points) of galvanic current without galvanic interaction. Separate calculation were first made for the Steel-Mg couple (i.e. connecting only the six steel and the six AZ91D plates on the left of the galvanic corrosion interaction specimen illustrated in Figure 5 to give the curve St_Mg and the data (Test 1SM and Test 2SM). Subsequently calculations and measurements were made for Mg_St by connecting the six AZ91D plates to the six steel plates on the right. $d = 10$ mm.

current distribution for the steel-AZ91D galvanic couple (curve St_Mg) without any galvanic interaction, and also (b) the AZ91D-steel galvanic couple (curve Mg_St) without any galvanic interaction. There was a good agreement between the BEM model and the experimental measurements for both cases (a) and (b). Figure 17 presents the curve "Addition" as the linear addition of the galvanic current for the AZ91D electrodes calculated for steel-AZ91D couple and AZ91D-steel couple, without galvanic interaction. The superimposed galvanic current for the AZ91D electrodes was in a reasonable agreement with the BEM model for the steel-AZ91D-steel galvanic interaction specimen. Figure 18 presents the addition of the measured galvanic current for the AZ91D electrode measured for the steel-AZ91D couple and for the AZ91D-steel couple, without galvanic interaction. Figure 18 also has the curve "Addition" from Figure 17 and the curve St_Mg_St from Figure 15. There was a reasonable agreement between

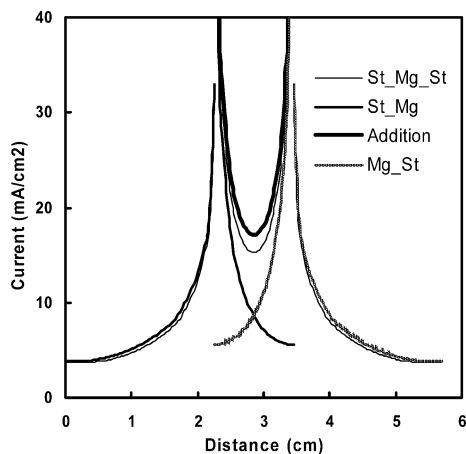


Fig. 17. Comparison of the BEM model of non-interacting galvanic current (St_Mg and Mg_St), interacting galvanic current (St_Mg_St) and linear addition of non-interacting galvanic current (curve "Addition").

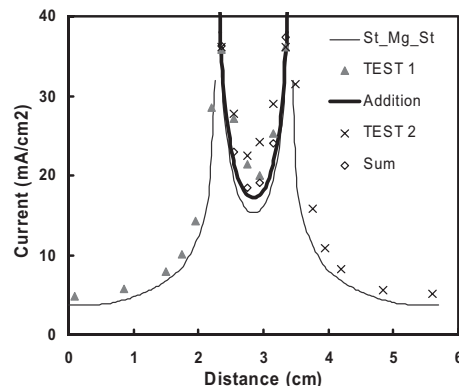


Fig. 18. Comparison of superposition of non-interacting galvanic current (curve "Addition"), interacting galvanic current (curve "St_Mg_St"), measured non-interacting galvanic current (data points from the Fig. 12) and linear addition of the measured non-interacting galvanic currents (data points designated as "Sum").

the linear addition of the experimental measurements and BEM calculations. This indicated that the current distribution for the AZ91D electrodes for galvanic interaction could be expressed as a linear superposition of the current caused by each individual galvanic couple.

Effect of Insulation Distance

Figure 19 illustrates the galvanic current distribution for the AZ91D-steel galvanic couple in 5% NaCl solution for various insulation distances $d = 0.5$ mm, 2.2 mm, 3.9 mm, 7.3 mm, 10.7 mm and 25 mm. The galvanic current of the AZ91D electrodes decreased as the insulating distance increased. The maximum galvanic current for the AZ91D electrode adjacent to the steel decreased significantly with the increase of the insulating distance. Furthermore, the total galvanic current for AZ91D electrodes decreased as the insulating distance increased. In another words, the increase of insulating distance leads to less galvanic corrosion attack both locally and totally. The influence of the insulating distance on the galvanic current distribution of steel electrodes was the same as that on the AZ91D electrodes. However, the magnitude of the influence on the steel electrodes was much smaller than that on the AZ91D electrodes. This BEM simulation was within expectations. It is also consistent with the results and the theoretical predictions of Song et al.^[15] The increase of the insulating distance increases the length of the circuit and thus increases the resistance of the circuit. Therefore the galvanic current of the adjacent anode and cathode decreases according to Ohm's law.

Steel Fastener

Figures 20 illustrates the physical appearance of the AZ91D plate after 48 hours immersion in 5% NaCl solution. The samples exhibited an unevenly distributed corrosion due to the galvanic couple with steel. Corrosion damage was deeper at the AZ91D-steel interface, and included pitting further away from the interface. Corrosion damage to AZ91D was concentrated around the steel and was largely confined to within about 1 to 2 cm radial distance from the interface. The radial

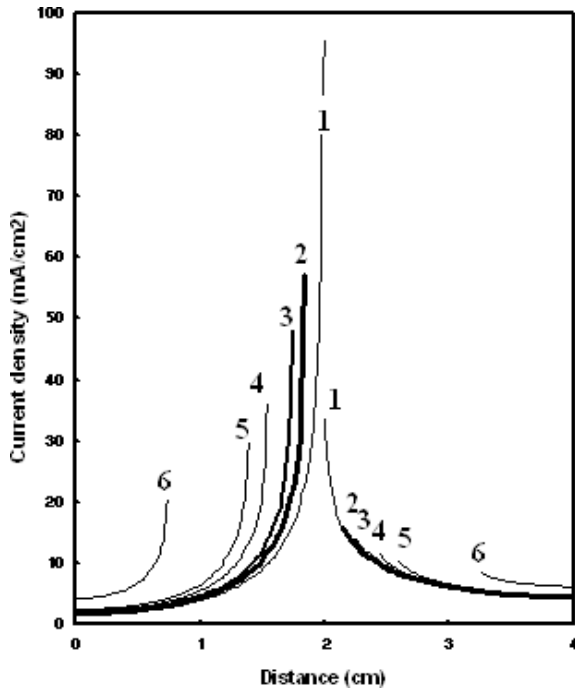


Fig. 19. Comparison of galvanic current distribution for the following distances, $d=0.5$ mm (Curve 1), $d=2.2$ mm (Curve 2), $d=3.9$ mm (Curve 3), $d=7.3$ mm (Curve 4), $d=10.7$ mm (Curve 5) and $d=25$ mm (Curve 6).

extent of the corrosion was similar in all these cases. There were some pits distributed randomly out on the remaining surface of the AZ91D. However, most of the remaining area was free from corrosion and retained its original appearance. This indicated that the effective distance of galvanic corrosion was limited to a distance of 1 to 2 cm. Most of the remaining area seemed to be protected as a cathode. A similar finding was also reported by Hawke,^[22] who derived an effective insulating space of about 5 mm for magnesium coupled with cast iron.

Comparison of the physical appearance of the corrosion with the area of galvanic corrosion as simulated by the BEM model showed that the computer model provided reasonable predictions of the effective galvanic corrosion area for each of the three different sizes of steel cathodes in 5% NaCl solution.

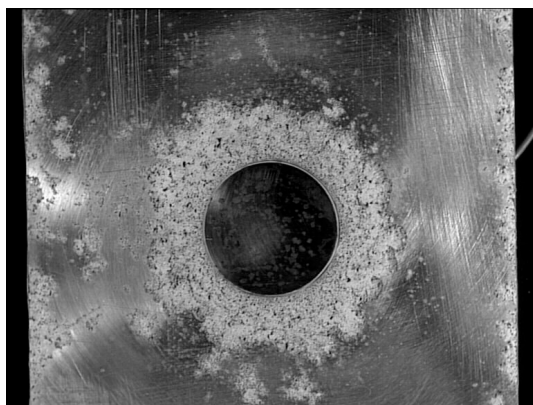


Fig. 20. Appearance of the fastener assembly (30 mm diameter steel cathode) after immersion in the 5% NaCl solution.

Figures 21 and 22 illustrate the typical distribution of total corrosion and provide a comparison between the total corrosion rate on the corroded area for each small cross section, and the galvanic current derived from the BEM modeling calculation for AZ91D coupled with a 10 mm diameter steel insert. The total corrosion rate for each small cross section was calculated from the corresponding measured corroded area. This total corrosion rate includes galvanic and self-corrosion, both of which may be in the form of pitting corrosion and general corrosion.

Analysis of the cross sectional damage indicated that the corrosion of AZ91D included unevenly distributed pitting corrosion. The maximum corrosion depth occurred close to but not always immediately adjacent to the magnesium-steel interface. A similar finding was also reported by Ault and Meany.^[53] The maximum depth occurred within about 1 mm away from the interface. The depth distribution of the galvanic pitting corrosion was quite randomly scattered on the surface and there was no obvious relationship between the depth and the pit location within a 2 cm distance.

Figure 22 illustrates the comparison of the BEM model predicted galvanic corrosion and the experimental measurement of the total corrosion for AZ91D coupled with a 10 mm steel insert. Both the BEM model and the experimental measurements indicate maximum corrosion at the magnesium-steel interface, and both indicated a decrease in corrosion rate with increasing distance from the interface. The experimental measurements indicate a corrosion rate significantly higher than the galvanic corrosion rate, and this is interpreted as self corrosion of magnesium. This self corrosion was estimated by subtracting the galvanic corrosion (as predicted by the BEM model) from the total measured corrosion. The value as estimated was ~ 10 mA/cm² at the magnesium-steel interface and similar values were estimated at a distance of 1 cm from the interface. This self corrosion corresponds to a penetration rate of ~ 230 mm/y.

Discussion

In 5% NaCl solution, the galvanic current was reasonably predicted by BEM based BEASY program for the AZ91D-steel couple. 5%NaCl solution is an aggressive environment and intense hydrogen revolution stirred up the corrosion product. The galvanic corrosion of AZ91 in 5% NaCl solution was unlikely to be interfered by the formation of a surface film. The galvanostatic polarization curve of AZ91D in 5% NaCl solution rapidly approached steady state, was in good agreement with the potentiodynamic polarization curve and was likely to be representative of the galvanic corrosion behavior of the AZ91D.

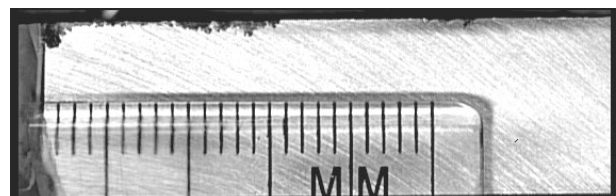


Fig. 21. Image of corrosion on Mg surface coupled with 10 mm diameter steel insert.

Conclusion

The BEM based BEASY program can reasonably predict the galvanic current distribution for AZ91D-steel in 5% NaCl solution.

The galvanic current distribution on AZ91D electrodes caused by galvanic interaction can be reasonably predicted as the linear superimposition of current of caused by each individual galvanic couple.

Both the BEM model and the experimental measurements of the galvanic corrosion of AZ91D coupled to steel predicted a similar distribution of the current density distribution: a maximum at the interface and decreasing rapidly to zero within 1 to 2 cm from the interface.

The total corrosion was interpreted as being due to galvanic corrosion plus self corrosion. The self corrosion was evaluated on the basis that the BEM model provides a good evaluation of the galvanic corrosion. On this basis, the self corrosion rate was evaluated to be typically ~ 230 mm/y for the area surrounding the interface and to a distance of about 1 cm from the interface.

Received: August 4, 2006

Final version: September 22, 2006

[1] G. Song, A. Atrens, *Adv. Eng. Mater.* **1999**, *1*, 11.
 [2] G. Song, A. Atrens, *Adv. Eng. Mater.* **2003**, *5*, 837.
 [3] N Winzer, A. Atrens, G. Song, E. Gahli, W. Dietzel, K. U. Kainer, N. Hort, C Blawert, *Adv. Eng. Mater.* **2005**, *7*, 659.
 [4] A. Atrens, *Adv. Eng. Mater.* **2004**, *6*, 83.
 [5] G. Song, D. StJohn, C. Bettles, G. Dunlop, *JOM* **2005**, *57*, 54.
 [6] G. Song, D. H. StJohn, *Corros. Sci.* **2004**, *46*, 1381.
 [7] G. Song, *Adv. Eng. Mater.* **2005**, *7*, 563.
 [8] G. Song, A. Atrens, S. StJohn, J. Nairn, Y. Lang, *Corros. Sci.* **1997**, *39*, 855.
 [9] G. Song, A. Atrens, D. StJohn, *Corros. Sci.* **1997**, *39*, 1981.
 [10] G. Song, A. Atrens, X. Wu, B. Zhang, *Corros. Sci.* **1998**, *40*, 1769.
 [11] G. Song, A. Atrens, M. Dargusch, *Corros. Sci.* **1999**, *41*, 249.
 [12] G. Song, D. StJohn, T. Abbot *Int. J. Cast Met. Res.* **2005**, *18*, 174.
 [13] G. Song, A. Bowles, D. StJohn, *Mater. Sci. Eng. A* **2004**, *74*, 366.
 [14] G. Song, D. StJohn *J. Light Met.* **2002**, *2*, 1.
 [15] G. Song, B. Johannesson, S. Hapugoda, D. H. StJohn, *Corros. Sci.* **2004**, *46*, 955.
 [16] D. Hawke, T. Ruden, *Soc. of Autom. Eng. [Spec. Publ.]* **1995**, *1096*, 63-7.
 [17] J. I. Skar, *Mater. Corros.* **1999**, *50*, 2.
 [18] G. Gao, in *The 2nd Isr. Int. Conf. on Magn. Sci. & Technol.* **2000**. Dead Sea, Israel.
 [19] H. O. Teeple, *AMS STP*, **1956**, *175*, 89.
 [20] G. Song, *Corros. Magn. Alloys*, PhD Thesis, **1997**, The University of Queensland, Brisbane. 178.
 [21] X. Wu, *Study on Corros. and Protection of Magn. Alloy*, PhD Thesis, *Inst. of Corros. and Protection of Met.* **1999**, Chinese Academy of Science: Shenyang China. 89.
 [22] J. I. Skar, *Mater. Corros.* **1999**, *50*, 2.
 [23] E Ghali, in *Magn. Alloys* **2000**, *350*, 261.
 [24] K. R. Baldwin, D. J. Bray, G. D. Howard, R. W. Gardiner, *Mater. Sci. Technol.* **1996**, *12*, 937.
 [25] G. L. Makar, J. Kruger, *Int. Mater. Rev.* **1993**, *38*, 138.
 [26] A. L. Olsen, *Metall.* **1992**, *46*, 570.
 [27] J. L. Genesca, L. Betancourt, C. Rodriguez, *Corros.* **1996**, *52*, 502.
 [28] V. Kaese, M. Niemeyer, P. Tai, J. Rottger, *Mater. Corros.* **1999**, *50*, 191.
 [29] J. T. Waber, *Corros.* **1957**, *13*, 95.
 [30] C. Wagner, *J. Electrochem. Soc.*, **1951**, *98*, 116.
 [31] J. R. Scully, H. P. Hack, *ASTM STP* **1988**, *978*, 136.
 [32] H. P. Hack, in *Galvanic Corros. Test and Standards Appl. and Interpretation*, **1995**, Fredericksburg, VA: American Society for testing and materials. 186-196.
 [33] V. Kucera, *Galvanic Corros. in the Atmos. Rapp. - Korrosionsinst.*, **1977**, 43.
 [34] F. Konig, M. Papke, *Mit Oberflaechentech.*, **1998**, *20*, 24.
 [35] H. Umehara, M. Takaya, T. Itoh, *Keikinzoiku*, **1999**, *49*, 172.
 [36] M. Isacson, M. Strom, H. Rootzen, O. Lunder, *SAE SP*, **1997**, *1250*, 43.
 [37] E. Boese, J. Gollner, A. Heyn, J. Strunz, C. Baierl, H. Schreckenberger, *Mater. and Corros.* **2001**, *52*, 247.
 [38] A. Tahara, T. Kodama, *Zairyo to Kankyo*, **1998**, *47*, 391.
 [39] R. A. Adey, S. M. Niku, *ASTM STP*, **1992**, *1154*, 248.
 [40] R. S. Munn, *ASTM STP* **1992**, *1154*, 215.
 [41] S. Aoki, K. Kishimoto, *Math. Comput. Modell.* **1991**, *15*, 11.
 [42] S. Aoki, K. Kishimoto, M. Miyasaka, *Corros.* **1988**, *44*, 926.
 [43] C. A. Brebbia, S. Walker, *Boundary Elements in Eng.* **1979**, Butterworth.
 [44] J. X. Jia, G. Song, A. Atrens, D StJohn, J. Baynham, G. Chandler, *Mater. Corros.* **2004**, *55*, 845.
 [45] K. Kishimoto, H. Miyasaka, S. Aoki, *JSME Int. J. Ser. I-Solid Mech. Strength of Mater.* **1989**, *32*, 256.
 [46] M. Miyasaka, K. Hashimoto, K. Kishimoto, S. Aoki, *Corros. Sci.* **1990**, *30*, 299.
 [47] W. Fischer, U. Hermann, M. Schroder, *Mater. Corros.* **1991**, *42*, 620.
 [48] F. E. Varela, Y. Kurata, N. Sanada, *Corros. Sci.* **1997**, *39*, 775.
 [49] H. P. E. Helle, G. H. M. Beek, J. T. Ligtelijn, *Corros.* **1981**, *37*, 522.
 [50] M. E. Orazem, *Corros.* **1997**, *53*, 264.
 [51] G. E. Strong, R. A. Adey, R. S. Rudas, in *13th Int. Corros. Congr.*, **1996**, Paper 56/1-Paper 56/6.
 [52] E. Bardal, R. Johnsen, P. O. Gartland, *Corros.* **1984**, *40*, 628.
 [53] J. P. Ault Jr. J. J. Meany, Jr., *12th Int. Corros. Congr.*, **1993**, *5A*, 3519.
 [54] J. W. Oldfield, *ASTM STP* **1988**, *978*, 5.
 [55] R. A. Adey, C. A. Brebbia, S. M. Niku, *Appl. of Boundary Elements in Corros. Eng.* **2002**.
 [56] W. E. Benbow, in *Iron and Steel*, Iliffe, London **1951**.
 [57] H. P. Hack, J. R. Scully, *Corros.* **1986**, *42*, 79.